Pergamon

Bioorganic & Medicinal Chemsitry, Vol. 2, No. 3, pp. 195-211, 1994

0968-0896/94 $6.00 + .00

0968-0896(94)E0009-Q

Theoretical Quantitative Structure–Activity Relationship Analysis On Three Dimensional Models Of Ligand–m1 Muscarinic Receptor Complexes

Francesca Fanelli,† M. Cristina Menziani,† Angelo Carotti‡ and Pier G. De Benedetti†*

†*Dipartimento di Chimica, Università di Modena, V. Campi 183, 41100 Modena, Italy*

‡*Dipartimento Farmaco-Chimico, Università di Bari, V. Orabona 4, 70125 Bari, Italy*

Abstract—The heuristic-direct QSAR (quantitative structure–activity relationships) approach has been applied to a series of 34 muscarinic receptor ligands, including antagonists, weak partial agonists, partial agonists and full agonists, interacting with the human m1-muscarinic receptor subtype. The first step of this procedure consists of the computer-aided 3D-model building of the receptor. The second step involves docking simulations with selected ligands, maximizing the complementarity between ligand and receptor. In the third step, a detailed and extensive correlation analysis between the computed interaction energies, their components and the experimental pharmacological affinity and action is accomplished in order to evaluate the consistency of the QSAR model proposed and to provide a quantitative tool for comparisons among the different complexes considered. In this context, good linear correlations have been obtained between ad hoc theoretical intermolecular interaction descriptors and the pharmacological action, which allow one to classify quantitatively and predict the pharmacological action of new ligands. Finally, according to the m1-receptor model proposed, it has been possible to speculate on the amino acid residues which are mainly involved in the interaction with the ligands, and on the nature of the prevailing intermolecular interactions which are responsible for the different behaviour of antagonists, weak partial agonists, partial agonists and full agonists.

Introduction

Theoretical QSAR (quantitative structure–activity relationships) analysis is now a well established tool which employs a large variety of theoretical molecular descriptors derived both from quantum mechanical calculations and computer assisted molecular modelling procedures, in order to rationalize the variation of the common bio-activity within an appropriate and informative set of molecules. This implies that the bio-activity is reduced and translated into the chemical formalism, through the maximization of the molecular complementarity between the ligand and the target of known three dimensional (3D) structure (direct approach or receptor fitting) or unknown 3D-structure (indirect approach or ligand fitting). In the first case, the ligand–target complementarity is explicitly taken into account by the modelling procedures, energetically optimizing the intermolecular interactions of the ligand–target complex. In the second one, a comparative analysis of the 3D-structural commonalities, differences and reactivity characteristics among an informative set of ligands allows the definition of a pharmacophoric moiety from which the complementary features of the receptor can be inferred. Hence, the main problem is to define and extract the most appropriate theoretical molecular descriptors ad hoc for the problem under study.[1]

Very recently, a third theoretical QSAR approach, named heuristic direct, in between the previous two, has been presented.[2] This approach, applicable when the atomic resolved structure of the target is unknown but predictable by means of the available experimental information, is able to handle the heterogeneous experimental data on the ligands and their targets and synthesize and translate them into QSAR models. This procedure is particularly useful for the study of the membrane-bound neurotransmitter receptors whose 3D-structure is not yet resolved at atomic level, but may be predicted by means of the relevant information obtained by cloning and sequencing experiments by biochemical and structure–activity relationships studies. The first step of this procedure consists of the computer-aided 3D-model building of the receptor. The second step involves docking simulations with selected ligands, maximizing the complementarity between ligand and receptor. In the final step, a detailed and extensive correlation analysis between the computed interaction energies, their components and the experimental binding affinities is accomplished in order to evaluate the consistency of the QSAR model proposed.

In this work, the heuristic-direct QSAR approach has been applied to a series of muscarinic receptor ligands. Muscarinic receptors belong to a large family of cell surface receptors which stimulate or inhibit specific intracellular signal transduction pathways, via coupling to guanine nucleotide regulatory proteins (G-protein coupled receptors, GPCRs).[3,4] Like all other GPCRs, muscarinic receptors are predicted to be composed of seven hydrophobic transmembrane helices (TMs) connected by alternating intracellular and extracellular loops, a glycosilated extracellular N-terminal domain and an intracellular C-terminal tail. Structure–function relationships of muscarinic drugs established that a cationic head group (usually a substituted ammonium moiety) is

*Author to whom correspondence should be addressed.

essential for strong muscarinic or antimuscarinic activity.[6] Mutagenesis as well as peptide labelling and sequencing studies of muscarinic receptors suggest that the binding of agonists and antagonists is initiated by an ion–ion interaction between the quaternary amine moiety of the ligands and an aspartic residue located in the TM 3 of the receptor proteins.[5,6] Molecular cloning studies have revealed the existence of five different muscarinic receptor subtypes (m1–m5), which show a high degree of sequence homology but differ in their ligand binding, functional properties and tissue distribution.[7,8] In general, m1, m3 and m5 are coupled to the triphosphoinositide (PI) breakdown in a variety of expression systems, while m2 and m4 are linked to the adenylate cyclase inhibition.[7,8] Three subtypes of muscarinic receptors, M_1, M_2, and M_3 have been pharmacologically identified by means of both functional and radioligand binding studies.[9] It is likely that the m1 sequence corresponds to that of the M_1 receptor, the m2 to the M_2 receptor and the m3 to the M_3 receptor.[10] The presence of both M_1 and M_2 receptors in rat cerebral cortex has been suggested, although it seems that the majority of the cortical muscarinic receptors are of the M_1 subtype.[11]

Several 3D-models of the muscarinic receptor TM domain based on the structure of bacteriorhodopsin were recently proposed.[12–16] A detailed qualitative description of the putative binding site interacting with the endogenous agonist was usually given.[12–14,16] Nordvall and Hacksell analyzed the interaction of ten structurally different agonists with the human m1-receptor binding site obtained by a combination of the homology-based and the indirect modelling procedures; however, their approach was primarily qualitative.[15]

We present, here, a quantitative description of the interaction of the human m1-receptor with a wide ranging and structurally heterogeneous molecular series of muscarinic ligands, including antagonists, weak partial agonists, partial agonists and full agonists (Scheme I).

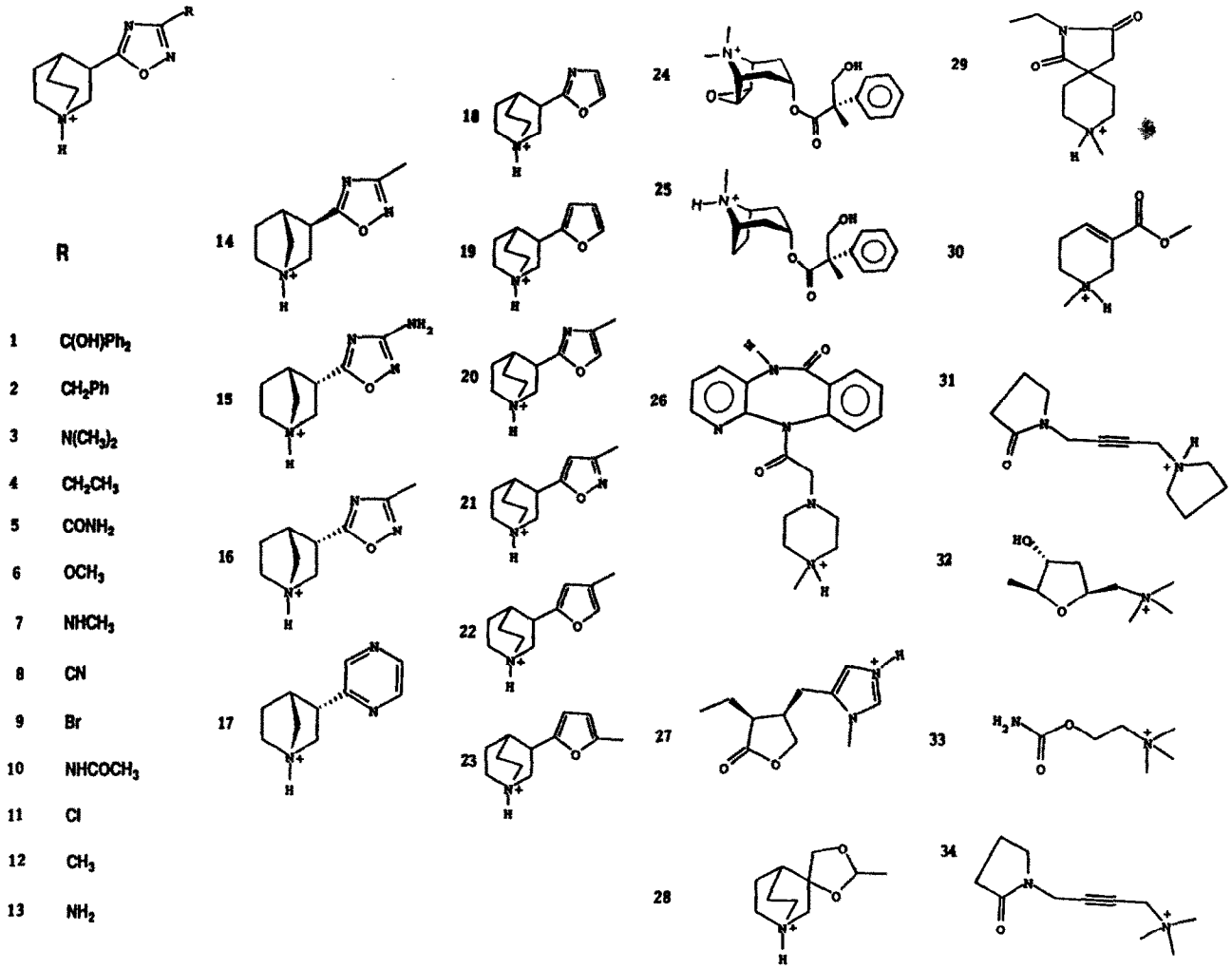

ANTAGONISTS: **1–3, 24–26**;
WEAK PARTIAL AGONISTS: **4–9, 18–23, 27–29**;
PARTIAL AGONISTS: **10–12, 30**;
FULL AGONISTS: **13–17, 31–34**.

Scheme I.

The 3D-model of the TM region has been built by taking the backbone coordinates of bacteriorhodopsin as initial template; moreover, the results obtained both from our previous theoretical indirect QSAR study on a set of 22 ligands[1] and from published site directed mutagenesis experiments[5,6] have been used in order to determine the binding preferences of the ligands. Our aims are: (a) to obtain quantitative correlations between ad hoc theoretical intermolecular interaction descriptors and the literature pharmacological affinity and action; (b) to identify the protein residues which, according to the theoretical model proposed, are mainly involved in the interactions with the ligands; and (c) to provide an additional tool based on comparative linear correlation analysis of the energy contributions of the amino acid residues mainly involved in the ligand binding, for elucidating the receptor structure–affinity relationships and suggesting future site-directed mutagenesis studies.

Results and Discussion

3D Model building

In the present study we have focused on the TMs of the receptor, which have been selected according to published sequence alignments.[13] The seven α-helices have been constructed with the ϕ and ψ angles characteristic of α-helices in a hydrophobic environment (ϕ = -59° and ψ = -44°).[17] We have used the helix backbone coordinates from bacteriorhodopsin structure as initial template for the packing of the helices. Bacteriorhodopsin is the only membrane embedded protein whose three-dimensional structure was determined to a sufficient detail by electron cryo-microscopy.[18] Recently, a novel mutagenesis approach was utilized to identify receptor intramolecular interactions.[19] The results indicate that specific amino acids in the seventh hydrophobic segment of the α_2 and β_2 adrenergic receptors lie adjacent to the first hydrophobic segment.[19] The arrangement of the TMs predicted by these experiments is similar to that found in bacteriorhodopsin.[18,19] Hence, we have primarily fitted the α-carbon atoms of each alpha-helix on the corresponding one in the Henderson 3D-model of bacteriorhodopsin. The helices have been rotated around their main axes in order to locate the residues conserved among the GPCRs family, or shown to be important for the ligand binding, in the inside of the receptor. In order to relieve the steric conflicts between the side-chains of the neighbouring TMs, we have performed manual rotations of the dihedral angles of the side-chains and small translations and rotations of the helices. After extensive energy minimization, applied to improve helix–helix packing contacts, a different arrangement of the helices of the ml-model with respect to that of bacteriorhodopsin has been found. This may be due to the different amino acid composition of the two structures and, in particular, to the different position of the conserved proline residues.[20] Very recently, the projection map of the GPCR bovine rhodopsin has been determined by electron crystallography of two dimensional crystals by Schertler *et al.*[21] This map suggests that the structure of bovine rhodopsin differs from that of bacteriorhodopsin; however, three-dimensional crystallographic data is required to determine the structure experimentally.[20]

Description of the minimized ml-model and comparison with site-directed mutagenesis experiment results

About 90% of the buried surface of the minimized ml-model is hydrophobic. Furthermore, the resulting hydrophobic moment for each helix is quite reasonable, being generally away from the bundle and directed toward the lipid side-chains.[22] All the conformations of the amino acid side chains, upon minimization, show agreement with the first or the second or the third most common conformations reported in the side-chain Ponder and Richards rotamer library.[23] Scheme II reports a classification of the amino acids of each helix of the ml-minimized model into three groups: (a) the side chains face the core of the TMs; (b) the side chains interact with those of the neighbouring TMs; and (c) the side chains are directed toward the lipid bilayer. The positions of each residue in the helix have been determined by means of the graphical analysis of the 3D-model and by measuring the angle between the direction in which each residue points (given by the vector from the helix axis to the Cβ atom) and the direction in which the nearest adjacent helix is located (given by the vector from the axis to one helix of its nearest neighbour).[24] In this context, angles ranging from -70° to -120° or from -70° to 70° or from 70° to 120° are associated to the three groups of residues, respectively. Agreement with the previously published models has been achieved for the location of the amino acid residues.[13–15] From an analysis of Scheme II it emerges that the seven helices have different degrees of exposure to the lipid surrounding the structure, according to the following order: helix 4 > helix 5 > helix 1 > helix 2 = helix 7 > helix 6 > helix 3, as indicated by the percentages of the residues directed toward the lipid bilayer, with respect to the total number of residues in the helix. This arrangement of the helices mostly agrees with Baldwin findings on the distinctive environments of the seven helices in GPCRs.[20]

Affinity labelling, peptide mapping and sequencing studies using mustard derivatives of the muscarinic antagonist propylbenzilcholine and the physiological agonist acetylcholine (ACh) as alkylating probes suggest that the positively charged ammonium group of muscarinic ligands is anchored, by ion–ion interaction, to the carboxylate side chain of an Asp residue present in TM 3 of the receptor molecule (Asp_{308}, in our model; the first digit corresponds to the helix and the next two digits indicate the position of the residue in the helix).[6] Consistent with this finding, replacement of the Asp_{308} with Asn resulted in a mutant receptor with drastically reduced binding affinities.[5,6] Sequence analysis shows that the TMs of all muscarinic receptors contain a series of conserved Ser, Thr, and Tyr residues most of which are not found in other GPCRs. In order to test the hypothesis that one or more of these conserved residues may be able to interact with the ligands by hydrogen bonding, a series of rat m3-muscarinic receptor single point mutants, in which the various OH-group containing amino acids were individually replaced with Ala (Ser, Thr) or Phe (Tyr), were created and

	HELIX 1	HELIX 2	HELIX 3	HELIX 4	HELIX 5	HELIX 6	HELIX 7
Side chains directed toward the TMs core	ILE102 THR113 VAL120[a]	LEU202 ASP209[a,c] SER216[a,c] TYR223	TRP304[b] ASP308[b,c] ALA311 ALA314 SER315[b] ASN318 ILE322	TRP406[a,c] TRP413[b] TRP420	THR503[b,c] VAL514	LEU602[b] LEU606[a] PHE609 TRP613[a,c] LEU621	VAL702 GLU704 GLU708 TYR715[b,c] THR719
Side chains interacting with those of the neighbouring helices	PHE101 THR105 THR106 LEU108 LEU109 SER110 ALA112 VAL114 GLY116[b] ASN117[a] LEU119[a] LEU121 SER123 PHE124	PHE201[b] LEU203 LEU205[a] ALA206[a] ALA208 LEU210[a] ILE212 GLY213 PHE215 MET217 LEU219 TYR220[c] THR222 LEU224	CYS301 LEU303 LEU305 LEU307 TYR309[b,c] VAL310 SER312 ASN313 VAL316[b] MET317 LEU319[a] LEU321	ILE402[a] ALA405 LEU407 SER409[b] PHE410 LEU412 ALA414 ALA416 ILE417 PHE419	PHE501 GLY502 ALA504[b] ALA506 ALA507[b] LEU510 PRO511[a,c] THR513 MET515 THR517 LEU518 ARG521	THR601 SER603 ILE605[a] LEU607 ALA608 ILE610 THR612 THR614 TYR616[a,c] ASN617[b] VAL620 VAL622	CYS701 THR705 TRP707 LEU709 TYR711[c] TRP712[b] CYS714 VAL716 SER718[b] ASN721[a] PRO722[a,c] MET723 TYR725[a]
Side chains directed toward the lipid bilayer	GLY103 ILE104 GLY107 LEU111 THR115 LEU118 ILE122 LYS125	SER204[b] CYS207 ILE211 THR214 ASN218 THR221 LEU225	ASP302 ALA306 LEU320	MET401 GLY403 LEU404 VAL408 VAL411 PRO415[a,c] LEU418 GLN421	MET505 PHE508[b] TYR509[b] VAL512 CYS516 TYR519[a] TRP520	ALA604 LEU611 PRO615[a,c] ILE618 MET619	PRO703 LEU706 GLY710 LEU713 ASN717[b] ILE720 CYS724

Scheme II. [a]Conserved in the GPCRs family. [b]Conserved in the cationic neurotransmitter GPCRs. [c]Shown to be important by site directed mutagenesis experiments.

pharmacologically characterized in radioligand binding studies.[6] Site directed mutagenesis experiments on the rat m3[6] demonstrated that the mutant receptors: Thr_{234} (Thr_{503}) → Ala (the mutated residue Thr_{234} in the rat m3 corresponds to the Thr_{503} in our model) and Tyr_{506} (Tyr_{616}) → Phe show about 30- to 40-fold lower binding affinities for the agonists ACh and carbachol binding than the wild-type receptor and also reduced potencies in ACh- and carbachol-induced stimulation of PI hydrolysis.[6] Moreover, these experiments showed that the mutation of these two residues does not influence or influences to a small extent the affinity of the antagonists *N*-methylscopolamine (NMS) and trihexylphenidyl binding, respectively.[6] In our model Thr_{503} and Tyr_{616} are located at the same level of the conserved Asp_{308}. Furthermore, Tyr_{148} → (Tyr_{309}) Phe, Tyr_{529} (Tyr_{711}) → Phe and Tyr_{533} (Tyr_{715}) → Phe mutants showed about 10-fold lower binding affinities for ACh, carbachol and about 3-fold lower affinities for the antagonists, NMS and trihexylphenidyl, than the wild-type receptor.[6] Amino acid replacements of residues buried deeper in the membrane such as Thr_{502} (Thr_{612}) and Thr_{537} (Thr_{719}) showed little

effect on agonist binding.[6] Furthermore, it was found that Ser_{120} (Ser_{216}) → Ala mutant binds both NMS and trihexylphenidyl with about 10-fold lower affinities than the wild-type receptor, whereas it does not affect agonist binding.[6] A recent mutagenesis study on the rat m3 also suggested that Pro_{201} (Pro_{415}), which is conserved among virtually all GPCRs, is essential for high-affinity ligand binding.[6] Helical wheel projection models predict that Pro_{201} (Pro_{415}) is located on the outside of the helical bundle, facing the lipid bilayer, indicating that this Pro residue might exert an indirect conformational effect that allows high affinity ligand binding.[25] In our model the location of Pro_{415} agrees with the prediction of the helical wheel projection model proposed by Hulme *et al.*[25] Site-directed mutagenesis experiments also demonstrated that the mutant receptors Trp_{192} (Trp_{406}) → Phe and Trp_{503} (Trp_{613}) → Phe show clearly reduced binding affinities for all the ligands investigated, indicating a possible involvement of these residues in the binding of agonists and antagonists.[6] Other site-directed mutagenesis experiments on the human m1 showed that the replacement of Tyr_{82} (Tyr_{220}) with a Phe, the corresponding residue in the m3, reduces the pirenzepine affinity by about 3-fold, accounting for part of the affinity shift between m1 and m3.[26] The affinities of the agonist carbachol and of the antagonist atropine are not influenced by this mutation.[26]

Docking experiments

We have performed docking simulations on 34 muscarinic ligands (Scheme I), which span the efficacy range from antagonists, through weak partial agonists and partial agonists to full agonists. We have started the docking experiments with the antagonist NMS (**24**) and the full agonist carbachol (**33**), since these are the ligands mainly utilized in the binding studies on mutant muscarinic receptors.[6,26] Site-directed mutagenesis studies suggest that the amine functions of agonists and antagonists are bound in much the same way but that the other molecular moieties recognize and bind different loci of the receptor. Overlapping but different binding sites for agonists and antagonists were also proposed in a modelling study on the β_2-adrenergic receptor.[27] Hence, we have docked both the ligands into the putative binding domain by using as molecular recognition and fitting criterion, the formation of an ion–ion interaction between the ligand quaternary ammonium head group and the carboxylate of Asp_{308}. The docking of the antagonist NMS and of the agonist carbachol has been repeated several times with different initial orientations of the ligand and of the side chains, in order to optimize (a) the ion–ion interaction between the ligand ammonium head group and the Asp_{308} for both the compounds, (b) the H-bonding interaction between the antagonist hydroxy group and Ser_{216}, (c) the H-bonding interaction between the agonist carboxy group and both Thr_{503} and Tyr_{616}, and (d) other interactions with amino acid residues shown to be important for the ligand binding.[6,26] The complexes obtained were energy refined. All the atoms of both the ligand and the receptor have been allowed to move during minimization. From the analysis of the two selected minimized complexes it emerges that the antagonist and the agonist binding domains are located about 14 Å and 11 Å below the extracellular surface, respectively, in agreement with recent fluorescence emission and quenching experiments.[28] On the basis of these considerations, we have extended the docking experiments to all the ligands listed in Scheme I. Antagonists and agonists have been docked in the same sites of NMS (**24**) and carbachol (**33**), respectively; the weak partial and partial agonists have been mainly fitted in between the antagonist and agonist domains, by shifting their orientation in one domain or in the other, depending on the relative values of the NMS/OXO-M affinity ratio (for the definition of this index see the binding assays section).[29] For each ligand the docking minimization has been repeated several times, according to the procedure used for NMS and carbachol. The main chain conformations and the packing of the seven helices, upon docking minimizations, show differences among the 34 selected ligand–receptor minimized complexes in relation to the nature of their intermolecular interactions. Moreover, the side chain conformations of these complexes are similar, except those of the residues directly involved in the interactions with the ligands and are in agreement with those tabulated by Ponder and Richards.[23]

Binding assays

Freedman *et al.* described a simple binding assay which predicts the efficacy of muscarinic compounds in rat cerebral cortex, using two well established radioligand binding assays.[11] The muscarinic antagonist [^{3}H]-*N*-methylscopolamine (NMS) was used to label both high affinity and low affinity states of the receptor, the muscarinic agonist [^{3}H]-oxotremorine-M (OXO-M) was used to label the high affinity agonist state of the receptor. In this way, it was possible to measure the affinity of a large number of compounds for either state of the receptor.[11,30] Since agonists recognize preferentially the high affinity state, displaying much higher affinity in the OXO-M binding assay with respect to the NMS assay, whereas antagonists show similar affinity in both assays, the ratio of the affinities of a given compound (NMS/OXO-M ratio) gives a measure of its cortical efficacy.[11] The log of this ratio has been shown to correlate directly to the ability of the ligand to stimulate the hydrolysis of cortical PI and thus its predictive value is assured.[11] Four broad categories of muscarinic ligands can be defined according to their efficacy as estimated from this ratio: antagonists show equal affinity in both binding assays and thus have ratios close to unity, weak partial agonists have low ratios between 10–200, partial agonists display intermediate ratios 200–800 whereas, at the other end of this continuum, full agonists display a ratio in excess of 800.[11,30]

QSAR and correlation analyses

Table 1 reports the experimental binding affinities p(NMS) and p(OXO-M), and the logarithm of their ratio: log(NMS/OXO-M) for the ligands listed in Scheme I.[11,30]

The interaction energy (*IE*, for the definition of this index see the experimental section) of the minimized ligand–m1-receptor complexes and their van der Waals (IE_{VDW}), H-

Table 1. Experimental binding affinities (p(NMS), p(OXO-M), log(NMS/OXO-M) and calculated theoretical intermolecular interaction descriptors (*IE*, IE_{VDW}, IE_{HB}, IE_{EL}, IE_{VDW}%, IE_{HB}%, IE_{EL}% and $IE_{(HB+EL)}$%).

N.	p(NMS)[a]	p(OXO-M)[a]	$\log\left(\frac{NMS}{OXO\text{-}M}\right)$[a]	IE[b]	IE_{VDW}[c]	IE_{HB}[c]	IE_{EL}[c]	IE_{VDW}%[c]	IE_{HB}%[c]	IE_{EL}%[c]	$IE_{(HB+EL)}$%[d]
1	9.92	10.17	0.25	-69.94	-57.06	-3.54	-9.34	81.58	5.06	13.35	18.41
2	7.15	7.68	0.53	-58.43	-47.18	-3.38	-7.87	80.75	5.78	13.47	19.25
3	6.70	7.68	0.98	-56.21	-43.62	-3.63	-8.96	77.60	6.46	15.94	22.40
4	7.02	8 25	1.23	-50.33	-38.41	-3.84	-8.08	76.32	7.63	16.05	23.68
5	4.41	5.77	1.36	-57.30	-39.69	-7.76	-9.85	69.27	13.54	17.19	30.73
6	6.28	7.85	1.57	-49.10	-37.53	-3.89	-7.67	76.43	7.92	15.62	23.54
7	5.70	7.28	1.58	-51.45	-37.13	-6.34	-7.97	72.17	12.32	14.63	27.81
8	5.58	7.37	1.79	-47.18	-34.55	-3.92	-8.71	73.23	8.31	18.46	26.77
9	6.72	8.96	2.24	-49.99	-34.26	-6.27	-9.46	68.53	12.54	18.92	31.47
10	4.64	6.92	2.28	-63.36	-42.31	-11.17	-9.88	66.78	17.63	15.59	33.22
11	6.72	9.32	2.60	-54.55	-36.34	-8.89	-9.32	66.62	16.30	17.08	33.38
12	6.35	9.04	2.69	-55.85	-37.61	-8.94	-9.29	67.34	16.01	16.63	32.64
13	6.22	9.30	3.08	-56.83	-35.85	-12.38	-8.60	63.08	21.78	15.13	36.92
14	7.00	10.00	3.00	-54.32	-35.44	-9.56	-9.31	65.24	17.60	17.14	34.74
15	5.75	8 85	3.11	-52.89	-31.02	-12.63	-9.24	58.65	23.88	17.47	41.35
16	5.44	8.68	3.24	-51.46	-33.36	-9.03	-9.06	64.83	17.55	17.60	35.15
17	5.80	9.15	3.35	-47.47	-31.09	-7.37	-9.01	65.49	15.52	18.98	34.51
18	5.17	7.42	2.25	-46.52	-33.23	-3.92	-9.36	71.43	8.43	20.12	28.55
19	5.48	7.47	1.99	-46.60	-34.31	-3.76	-8.53	73.63	8.07	18.30	26.37
20	5.85	7.57	1.72	-50.10	-37.76	-3.70	-8.64	75.37	7.38	17.24	24.63
21	5.85	7.44	1.59	-50.38	-37.64	-3.51	-9.23	74.71	6.97	18.32	25.29
22	5.85	7.24	1.40	-50.57	-38.36	-3.58	-8.63	75.85	7.08	17.06	24.14
23	6.60	7.89	1.29	-49.09	-37.38	-3.49	-8.21	76.14	7.11	16.72	23.83
24	9.55	9.66	0.11	-61.01	-50.79	-3.09	-7.13	83.25	5.06	11.69	16.75
25	9.00	9.32	0.32	-59.22	-47.93	-3.49	-7.80	80.93	5.89	13.17	19.06
26	7.14	7.48	0.34	-69.36	-53.60	-6.78	-8.98	77.28	9.77	12.95	22.72
27	5.40	7.40	2.00	-51.50	-39.54	-4.27	-7.69	76.78	8.29	14.93	23.22
28	5.31	7.45	2.14	-48.22	-35.87	-3.31	-9.02	74.39	6.86	18.70	25.57
29	5.30	7.40	2.10	-55.63	-41.89	-6.38	-7.35	75.30	11.47	13.21	24.68
30	5 21	7.96	2.75	-43.41	-28.91	-6.86	-7.63	66.60	15.80	17.58	33.38
31	6.08	9.02	2.94	-56.81	-39.05	-10.03	-7.72	68.74	17.65	13.59	31.24
32	4.72	8.32	3.60	-54.14	-36.37	-6.65	-12.12	67.18	12.28	22.39	34.67
33	4.62	8.24	3.62	-47.07	-29.24	-9.77	-8.06	62.12	20.76	17.12	37.88
34	5.66	9.28	3.62	-53.78	-38.86	-7.28	-7.64	72.26	13.54	14.21	27.74

[a]Refs. 11 and 30. [b]*IE* is the interaction energy (kcal/mol) of the minimized ligand–receptor complexes. [c]IE_{VDW}, IE_{HB}, IE_{EL} are the van der Waals, H-bonding and electrostatic energy components (kcal/mol) of the total *IE* and IE_{VDW}%, IE_{HB}%, IE_{EL}%, are the percentage contributions with respect to *IE*. [d]$IE_{(HB+EL)}$% are the percentage of the H-bond plus the electrostatic contributions with respect to *IE*.

bonding (IE_{HB}) and electrostatic (IE_{EL}) energy components, are also reported in Table 1, together with their percentage contributions with respect to *IE* and the percentage of the H-bond plus the electrostatic contributions ($IE_{(HB+EL)}$%).

It was demonstrated that in binding studies using antagonists as radioligand (i.e. [^{3}H]-*N*-methyl-scopolamine), displacement curves with muscarinic antagonists and weak partial agonists have Hill (N_H) coefficient close to 1.0, whereas muscarinic agonists yield Hill coefficient significantly less than 1.0 (N_H closer to 0.5).[11] Non linear regression analysis of such curves indicates that muscarinic agonists show a significantly better fit to a two site rather than to a single site model, with high and low-affinity binding components.[11] In agreement with these results, by plotting the total *IE* of the selected antagonist- and weak partial agonist–receptor complexes against the affinity constant p(NMS) (Figure 1a), a linear trend is achieved. The antagonist pirenzepine (**26**) whose N_H is close to 0.6 has been omitted. Furthermore, it was also shown that in binding studies using the agonist [^{3}H]-oxotremorine-M as radioligand, antagonists, weak partial agonists as well as full agonists display Hill coefficients close to 1.0.[11] In agreement with these results, by plotting the total *IE* values against the affinity constant p(OXO-M) (Figure 1b) a linear trend is obtained by considering all the categories of muscarinic ligands together. Again, the antagonist pirenzepine (**26**) showing N_H close to 0.6 has been omitted. The experimental conditions were chosen to maximize the difference between antagonists and agonists as displacing ligands,[11] as a consequence, the ratios of the affinity constants for the two binding assays (NMS/OXO-M) are used for predicting the cortical muscarinic efficacy.[11] Theoretical indices able to predict the cortical muscarinic efficacy in a similar manner as the NMS/OXO-M ratio, were defined in our previous indirect QSAR study on a series of quinuclidine-based derivatives, including compounds **1–13** and **18–23** of Scheme I.[1] Good

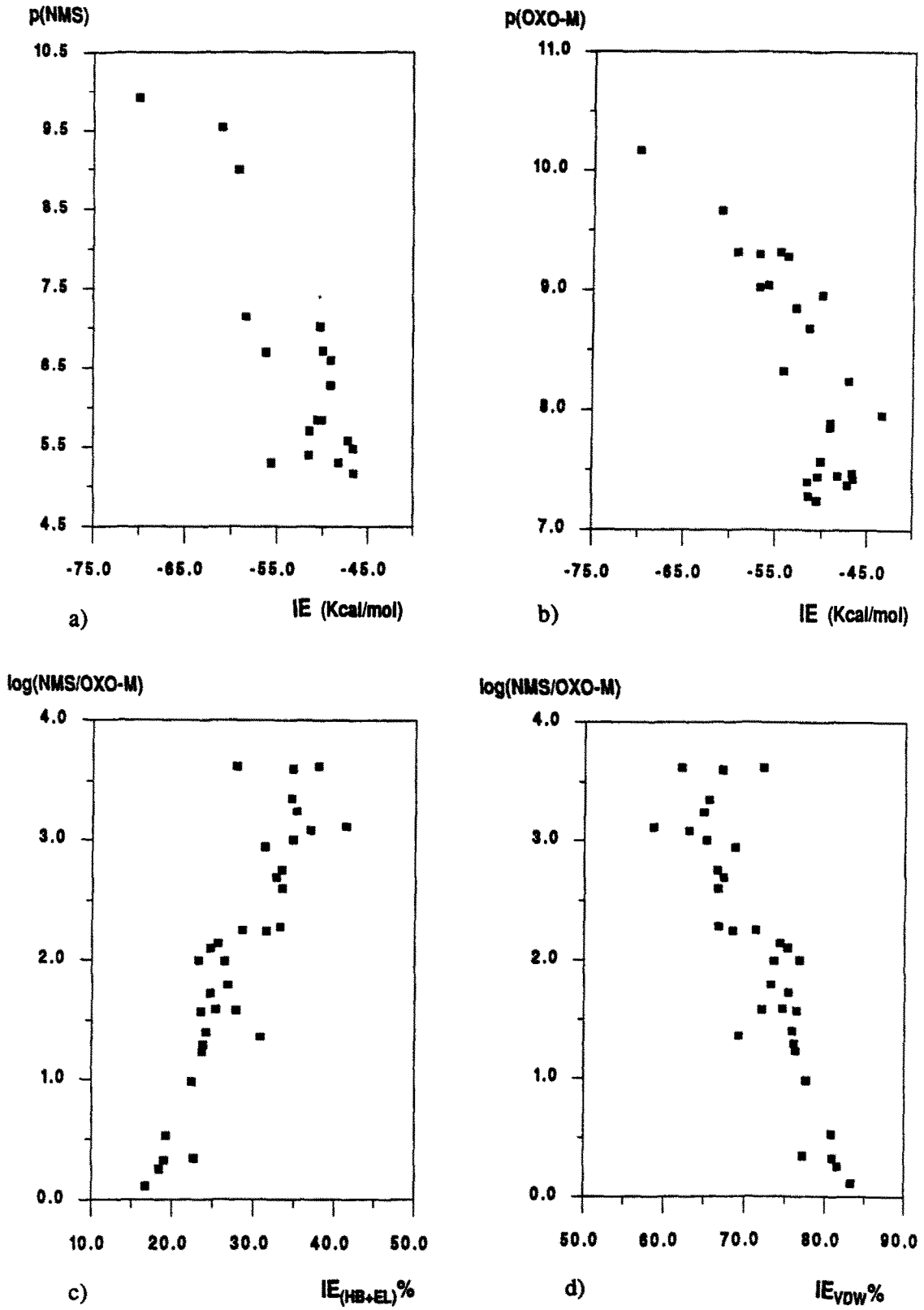

Figure 1. Correlations between the cortical muscarinic efficacy (log(NMS/OXO-M)), the dissociation constants for the muscarinic receptor in rat cortical membranes (p(NMS) and p(OXO-M)) and the theoretical intermolecular interaction descriptors $IE_{(HB+EL)}$%, IE_{VDW}% and *IE*. The linear regression equations are: (a) p(NMS) = -4.192 (±1.662) – 0.204 (±0.031)*IE*, n = 19 (omitted **5**, **10**, and **26**), r = 0.844, s = 0.797, r_{cv} = 0.807; only the antagonists and the weak partial agonists (log(NMS/OXO-M) values ranging form 1 to 2.3) have been considered; (b) p(OXO-M) = 1.724 (±1.058) – 0.126 (±0.021)*IE*, n = 25 (omitted **2**, **3**, **4**, **5**, **10**, **14**, **17**, **26** and **29**), r = 0.795, s = 0.552, r_{cv} = 0.753; (c) log(NMS/OXO-M) = -2.091 (±0.418) + 0.146 (±0.014)$IE_{(HB+EL)}$%, n = 34, r = 0.872, s = 0.512, r_{cv} = 0.854; log(NMS/OXO-M) = -2.155 (±0.346) + 0.147 (±0.012)$IE_{(HB+EL)}$%, n = 33 (omitted **34**), r = 0.910, s = 0.424, r_{cv} = 0.895; (d) log(NMS/OXO-M) = 12.555 (±1.081) – 0.146 (±0.015)IE_{VDW}%, n = 34, r = 0.865, s = 0.524, r_{cv} = 0.847; log(NMS/OXO-M) = 12.537 (±0.907) – 0.147 (±0.012)IE_{VDW}%, n = 33 (omitted **34**), r = 0.903, s = 0.439, r_{cv} = 0.888; n is the number of compounds, r is the correlation coefficient, s is the standard deviation, the numbers in parentheses give the 95% confidence intervals and r_{cv} is the crossvalidated r.

linear relationships, with positive slope, between the log(NMS/OXO-M) and the electrophilic superdelocalizabilities of the heterocyclic nitrogen atoms were obtained for compounds **1**–**13**; these molecular orbital (MO) indices may be considered as a theoretical measure of the hydrogen bonding acceptor propensity of the nitrogen atoms.[1] Furthermore, a good linear relationship, with negative slope, between the log(NMS/OXO-M) and the summation over the absolute values of the total net charges of all atoms of the heterocyclic substituent R and the heterocyclic ring ($|\Sigma q|$) was obtained; this index, being proportional both to the van der Waals volume of the substituent R and to the molecular polarization,[31] can be considered to describe the dispersion forces which are mainly operative in the hydrophobic environment. These results are in agreement with the pharmacophoric model proposed by Saunders *et al.*[32] for the same series of compounds which suggests that, once the essential charge reinforced H-bonding interaction between the protonated quinuclidine nitrogen atom and a protophilic counterpart in the receptor is satisfied, different modes of interaction become operative to differentiate among agonists, partial agonists and antagonists. In fact, full agonists utilize two H-bonding interactions to bind to the receptor and, in general, are small hydrophilic species; antagonists require maximally one and possibly no, H-bonding sites and instead utilize lipophilic interactions to stabilize the binding to the receptor; in between are partial agonists.[32] On these bases, we have defined herein $IE_{(HB+EL)}\%$ and $IE_{VDW}\%$ as ad hoc theoretical intermolecular interaction descriptors, useful for discriminating among antagonists, weak partial agonists, partial agonists and full agonists, in a similar manner with respect to the experimental NMS/OXO-M ratio. In fact, antagonists, like NMS (**24**), show $IE_{(HB+EL)}\%$ values below or close to 20% ($IE_{VDW}\%$ values above or close to 80%), full agonists, like carbachol (**33**), show $IE_{(HB+EL)}\%$ values above 30% ($IE_{VDW}\%$ values below or close to 65%), weak partial and partial agonists show $IE_{(HB+EL)}\%$ (or, complementary $IE_{VDW}\%$ values) in between the previous two. The consistency achieved between the theoretical intermolecular interaction descriptor $IE_{(HB+EL)}\%$ and the pharmacological action (log(NMS/OXO-M)), is shown by the good linear trend reported in Figure 1c. A similar relationship with opposite slope is obtained by plotting $IE_{VDW}\%$ against the log(NMS/OXO-M) (Figure 1d). Therefore, given the highly heterogeneous set of compounds considered, the theoretical intermolecular interaction descriptors $IE_{(HB+EL)}\%$ and $IE_{VDW}\%$ allow a generalization of the results obtained by means of the MO indices, electrophilic superdelocalizability and $\Sigma|q|$ respectively, computed on a congeneric series of compounds.[1]

In order to identify the amino acid residues of the proposed m1-model mainly involved in the interaction with the ligands, we computed the energy contributions of each residue to the total interaction energies of the selected minimized ligand–receptor complexes (Table 2). Figure 2 shows the complexes between the antagonist NMS (**24**, left side), the agonist carbachol (**33**, right side) and the TM α-carbon atoms of the human m1-muscarinic receptor. In deeper detail, Figure 3 shows a schematic representation of some ligands and the m1-receptor residues which are mainly involved in their binding interactions. By superimposing the interacting receptor residues in the same conformations and position they assume in the selected minimized complexes with the ligands, we have obtained the models of the binding domains of the antagonists (Figure 4a), weak partial agonists (Figure 4b), partial agonists (Figure 4c) and full agonists (Figure 4d).

From an inspection of the data values reported in Table 2, together with the graphical analysis of Figures 3 and 4, it emerges that Ser_{216} is involved in interactions with only the antagonists. In our interaction model it acts as H-bonding acceptor with respect to the hydroxy group of NMS (**24**, Figure 3), according to the results of site-directed mutagenesis which showed that antagonist binding significantly decreases on mutating this residue, whereas agonist binding is poorly affected.[6] Tyr_{220} acts as H-bonding donor with respect to the endocyclic carbonyl group of pirenzepine (**26**, Figure 3), according to site-directed mutagenesis studies.[26] Trp_{304} is involved in the interaction with antagonists and with some weak-partial agonists. By considering only the ligands which interact with Trp_{304} (Table 2), it emerges that the *IE* of Trp_{304} gives a linear trend with the total *IE* ($r = 0.81$, omitted **1**, **10** and **26**), showing that this residue may act as modulator of the ligand–receptor interaction energy. In our model this residue makes van der Waals attractive interactions with the quinuclidine moiety of compounds **1** and **2** (Figure 3), with the ammonium methyl groups of NMS (**24**, Figure 3), with the bicyclic moiety of atropine (**25**), with the piperazine ring of pirenzepine (**26**, Figure 3) and with the oxadiazole substituent of compounds **3**, **4**, **8**, **9**, and **10**. Trp_{304} also makes van der Waals attractive interactions with the aromatic heterocyclic moiety of the weak partial agonists **18**,**22** and with the ethyl group of RS86 (**29**, Figure 3). Asp_{308} gives the strongest, but nearly constant, contribution to the total *IE*, when it makes charge reinforced H-bonding interactions with the protonated nitrogen atom of the ligands. The *IE* of Asp_{308} gives a good linear trend with that of Thr_{503} ($r = -0.93$, omitted **27**, **33** and **34**); the negative slope of this correlation may suggest that the interaction of a ligand with one of these two residues negatively influences the interaction with the other one. In the interaction model proposed, Trp_{413} makes van der Waals attractive interactions with the molecular moieties directly bound to the protonated or quaternary nitrogen atom (Figure 3) for antagonists, partial agonists and full agonists, while, in the case of weak partial agonists, it makes π–π stacking interactions with the heterocycle bound to the quinuclidine moiety (**2**–**10**, **18**–**23**) or van der Waals attractive interactions with the substituent of the ring which contains the protonated nitrogen atom (**27**–**29**, Figure 3). Thr_{503} makes interactions with all the ligands, except for the antagonists, according to site directed mutagenesis experiments which indicated that the mutation of Thr_{503} with an Ala residue negatively affects both the affinity and the efficacy of ACh and of carbachol, while it does not affect the affinity of the antagonist NMS.[6]

Table 2. Energy contributions (kcal/mol) to the total *IE* of the human m1-muscarinic receptor residues interacting with the ligands considered.

N.	SER216	TYR220	TRP304	LEU307	ASP308	VAL310	SER409	PHE410	TRP413	THR503	ALA504	ALA507	TRP613	TYR616	ASN617	GLU708	TYR711	TRP712	TYR715
1			-1.02	-4.60	-14.00	-3.32			-1.55				-4.92	-2.56		-5.23	-6.47	-4.91	-4.06
2		-2.43	-3.21	-3.52	-11.92	-1.42			-3.95				-3.83		-2.05	-4.30	-5.60	-3.30	
3			-2.71	-1.02	-15.11		-3.03	-2.00	-5.67	-2.15		-1.06	-2.36		-3.79	-3.31	-4.01		
4			-2.12		-15.02		-3.17	-1.77	-5.39	-2.15		-1.07	-2.30		-3.96		-1.55		
5					-14.58		-4.44		-4.08	-1.67			-2.05	-3.80	-2.18	-2.50	-8.32	-1.30	
6					-15.08		-3.21	-1.75	-5.58	-2.03			-2.36	-3.10	-4.04		-1.55		
7					-14.97		-3.19	-1.72	-5.58	-2.04			-2.31	-5.27	-3.85		-1.47		
8			-2.32		-15.02		-3.55	-1.38	-4.48	-2.00			-2.67	-1.71	-3.75				
9			-2.80		-14.57				-4.30	-1.52			-2.40	-1.86	-5.97		-2.59		
10			-7.71		-14.96		-3.40		-5.66	-1.89			-2.46		-2.88	-2.46	-7.24		
11					-13.46				-6.01	-4.71			-5.47	-2.54	-6.21		-3.28		
12					-13.32				-6.00	-4.87	-1.78		-5.41	-2.59	-6.53		-3.24		
13					-13.35				-6.13	-5.87			-5.13	-3.46	-7.59		-3.49		
14					-13.21				-4.85	-5.37	-1.53	-1.76	-5.15	-2.43	-6.89		-2.21		
15					-13.19		-2.69		-3.88	-5.84		-1.59	-4.29	-1.70	-8.66				
16					-13.25		-2.64		-4.97	-4.82		-1.97	-4.29	-1.68	-6.02				
17					-12.15		-3.07		-4.50	-6.78		-1.18	-3.27	-1.27	-4.85				
18			-2.13	-1.10	-14.80		-3.44		-5.04	-1.72			-2.60	-1.32	-2.79	-2.65	-2.06		
19			-1.29		-14 48		-3.28	-1.74	-5.06	-2.54			-2.06	-2.12	-3.85		-1.64		
20			-1.87		-14.49		-3.21	-1.85	-5.37	-2.35		-0.90	-2.06	-2.74	-3.92	-2.44	-1.62		
21			-1.99		-14.74		-3.35	-1.77	-5.47	-2.40			-2.02	-2.48	-3.65	-2.79	-1.77		
22			-2.03		-14.52		-3.24	-1.87	-5.43	-2.50			-2.08	-2.64	-3.70	-2.48	-1.71		
23					-14.48		-2.99	-2.05	-5.39	-2.57			-2.32	-2.67	-4.23		-1.54		
24	-5.06	-3.23	-3.14	-4.57	-6.02	-3.01			-2.20				-1.92	-3.60		-7.14	-3.79	-2.82	-3.61
25		-2 47	-3.53	-4.93	-12.36	-2.09			-3.03				-1.80	-3.82		-6.57	-3.43	-2.93	
26	-1.18	-8.83	-1.21	-3.77	-15.07	-3.79			-2.09				-1.80	-2.35	-0.62	-4.71	-4.15	-2.50	-3.19
27					-11.53		-3.41	-1.50	-6.05	-2.12			-4.54	-4.12	-3.88	-0.06	-3.69		
28					-13.50		-3.80		-5.04	-2.29			-3.01	-3.41	-4.35	-1.33	-2.53		
29			-2.23	-1.43	-16.19		-2.71	-1.56	-5.88	-1.24			-3.29	-3.78	-5.63	-1.56	-2.21		
30					-11.58		-2.16		-4.64		-1.10	-1.62	-3.39	-2.24	-6.17		-2.50		
31					-11.24		-2.62		-3.03	-7.58	-1.37	-1.93	-4.26		-6.74		-2.48		
32					-9.27		-3.97	-2.78	-4.14	-8.59	-1.10		-1.90	-5.52	-5.85				
33					-6.76		-2.38		-5.20	-8.48			-1.74	-6.76	-4.97		-1.79		
34					-6.58		-2.68		-3 72	-7.58	-1.53	-1.60	-3.97	-2.47	-7.41		-2.89		

Figure 2. Side view of the complexes between NMS (**24**, left side), carbachol (**33**, right side) and the transmembrane backbone α-carbon atoms of the human m1-muscarinic receptor, in a direction perpendicular to the main axes of the seven α-helices. As for the proteins, the selected colours are: blue, pink, green, white, yellow, light blue, and violet, for helix 1, helix 2, helix 3, helix 4, helix 5, helix 6 and helix 7, respectively.

The *IE* of Thr_{503} gives a good linear trend with log(NMS/OXO-M) (r = -0.87); this correlation indicates that this residue acts as modulator of the pharmacological action. In our interaction model, Thr_{503} acts as H-bonding donor with respect to one of the two oxadiazole nitrogen atoms of compounds **11–17**, with the carbonyl oxygen atom of oxotremorine (**31**, Figure 3) and of oxotremorine-M (**34**) with the endocyclic oxygen atom of muscarine (**32**, Figure 3) and, finally, with the ester oxygen atom of carbachol (**33**, Figure 3). Trp_{613} makes van der Waals attractive interactions with all the ligands, mainly involving the groups directly bound to the protonated or to the quaternary nitrogen atoms, according to the results of site directed mutagenesis experiments.[6] Tyr_{616} gives van der Waals attractive interactions with most of the ligands, acting as H-bonding donor with respect to the carbonyl oxygen atom of carbachol (**33**, Figure 3), and as H-bonding acceptor with respect to the hydroxyl group of muscarine (**32**, Figure 3), according to the results of site directed mutagenesis studies.[6] Asn_{617} interacts with most of the ligands. Interestingly, the *IE* of Asn_{617} gives linear trends with the p(OXO) (r = -0.81, omitted **26**) and with the log(NMS/OXO-M) (r = -0.78); the latter correlation shows that this residue acts as modulator of the pharmacological action. It is worth noting that Asn_{617} is conserved among the muscarinic receptor subtypes and is substituted by a phenylalanine in the adrenergic receptors, whose natural agonists have an aromatic ring instead of the ACh ester function. In our interaction model Asn_{617} acts as H-bonding donor with respect to one of the two oxadiazole nitrogen atoms of **9**, **11–17**, with one carbonyl oxygen atom of RS86 (**29**, Figure 3), of arecoline (**30**, Figure 3), of oxotremorine (**31**, Figure 3) and of oxotremorine-M (**34**). Glu_{708} mostly makes a network of intramolecular H-bonds with Tyr_{223}, Trp_{304}, Tyr_{616} and Tyr_{711}; we have observed that Asp_{308} participates in this network when it does not interact with the ligands. Tyr_{711} makes van der Waals attractive interactions with most of the ligands, according to site directed mutagenesis experiments.[6] The *IE* of Tyr_{711} gives a good linear trend with the total *IE* (r = 0.81, omitted **5** and **26**), acting as modulator of the ligand–receptor interaction energy. Finally, Trp_{712} and Tyr_{715}, interacting with only the antagonists, belong to and define the accessory antagonist binding site.

In summary, from the analysis of the ligand–m1 interacting models previously reported, some conclusions can be drawn.

(a) Trp_{304} and Tyr_{711} act as modulators of the ligand–receptor interaction energy. Asn_{617} acts as modulator of the binding affinity constant p(OXO-M). Thr_{503} and Asn_{617} act as modulator of the pharmacological action.

(b) The protonated or quaternary nitrogen atom of the antagonists interacts with Asp_{308}, and it is surrounded by Trp_{304}, Trp_{413}, Trp_{613}. The other molecular moieties of the antagonists occupy the binding pocket mainly formed by the amino acid side chains of helices 2 and 7, such as: Ser_{216}, Tyr_{220}, Glu_{708}, Tyr_{711}, Trp_{712} and Tyr_{715}; these residues, with the exception of Glu_{708} and Tyr_{711} are not involved in the binding with the other ligands.

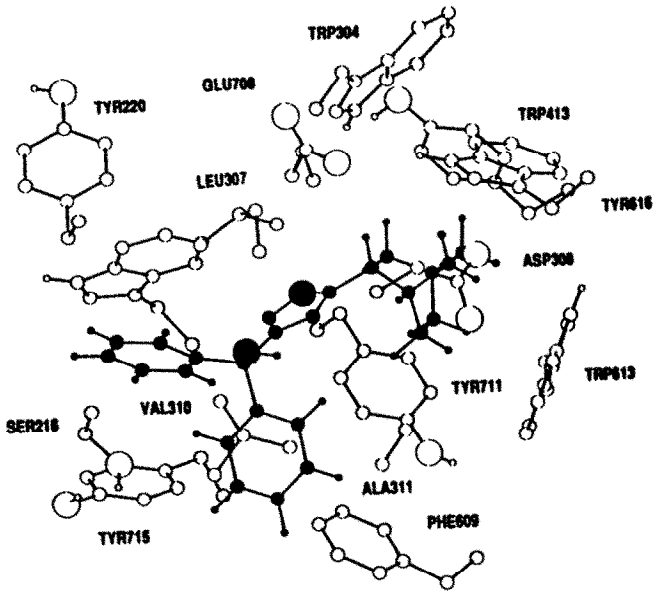

1

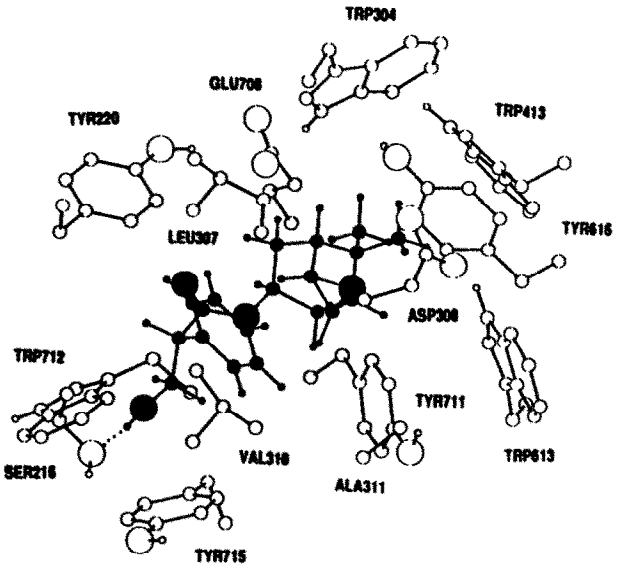

24

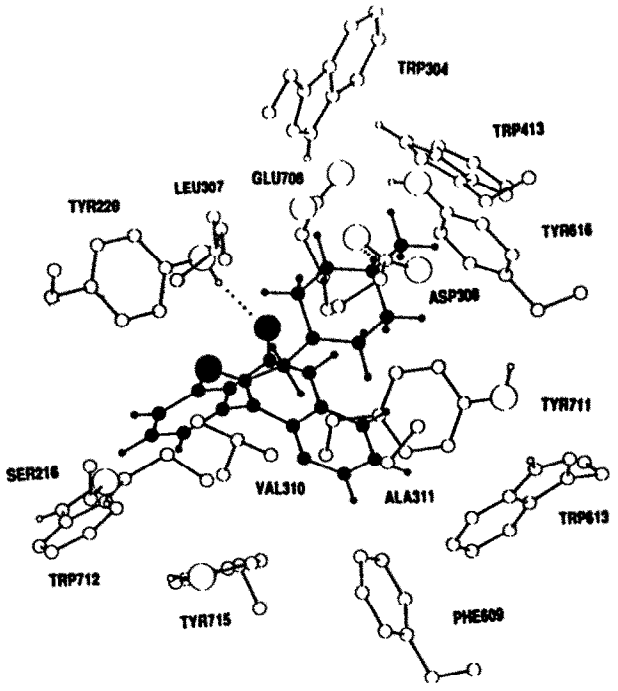

26

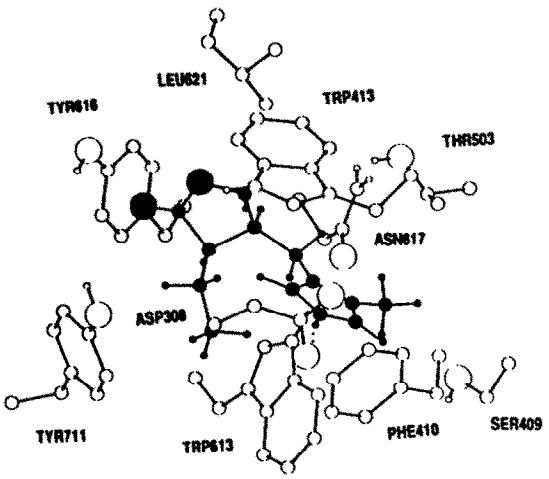

27

Figure 3.

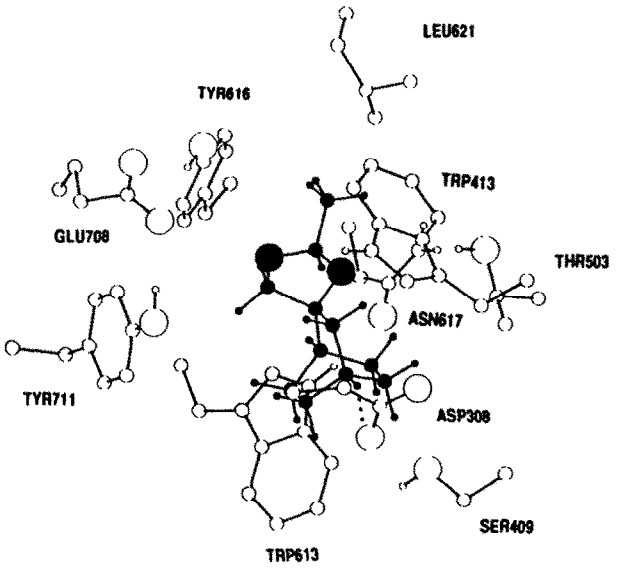

28

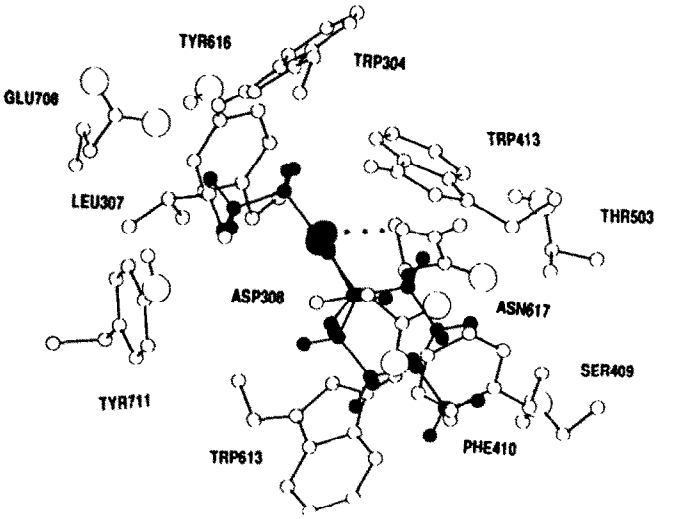

29

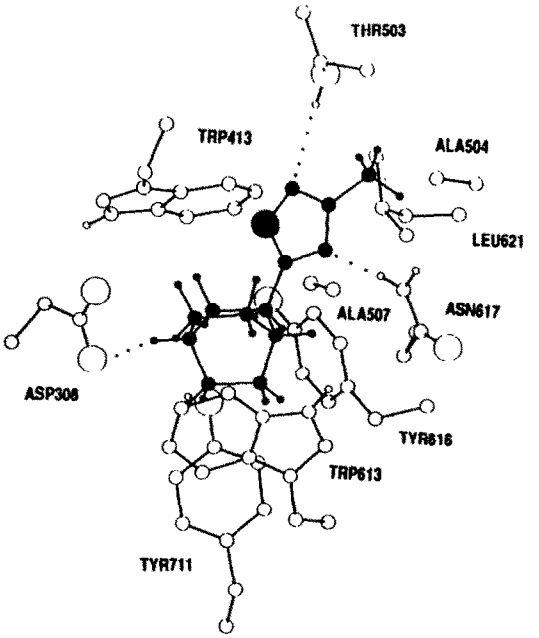

12

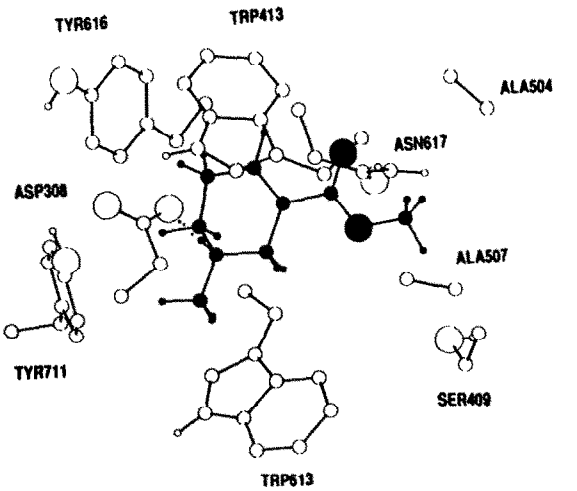

30

Figure 3. *Continued.*

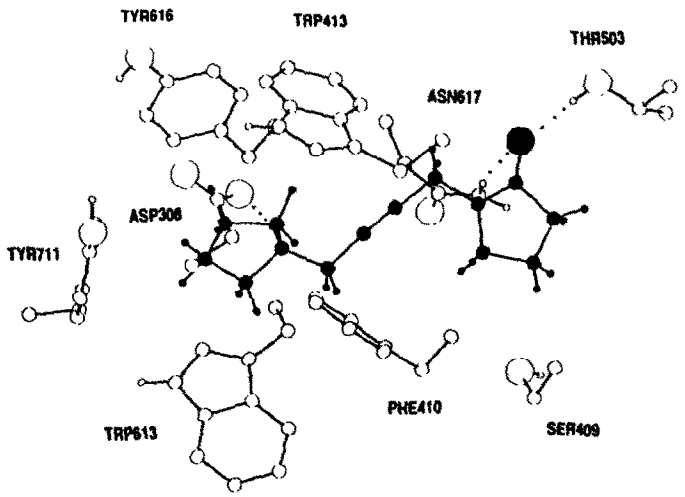

31

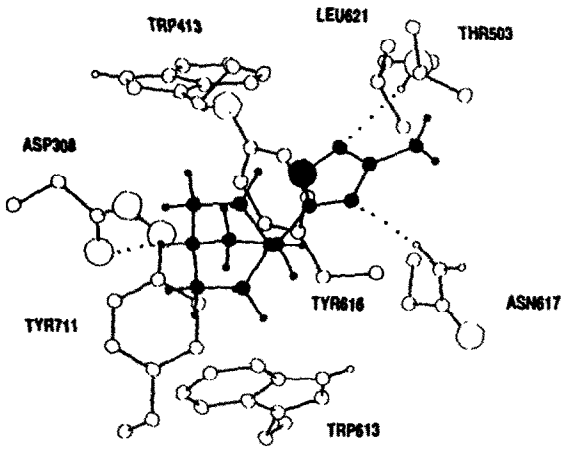

13

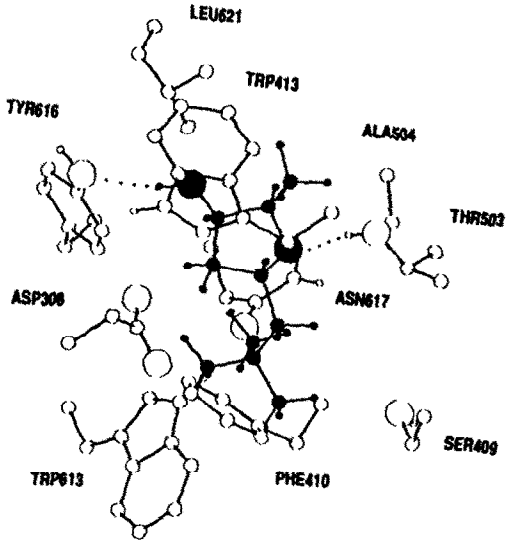

32

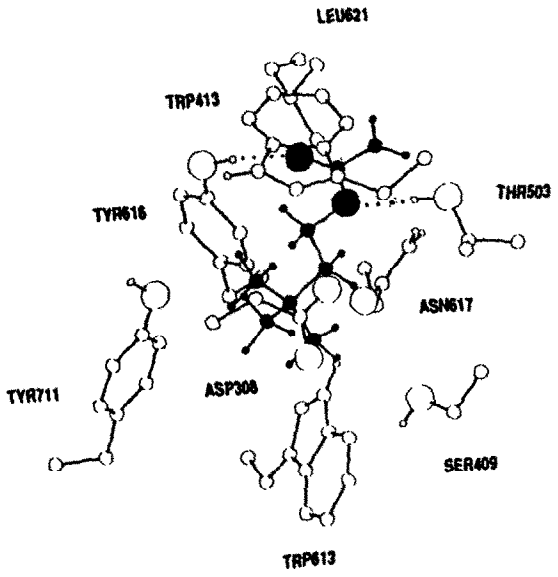

33

Figure 3. Schematic representation of some complexes between the ligands (antagonists: **1**, **24** and **26**; weak partial agonists: **27**, **28** and **29**; partial agonists: **12**, **30** and **31**; and full agonists: **13**, **32** and **33**) and the m1-receptor residues which contribute to the interaction.

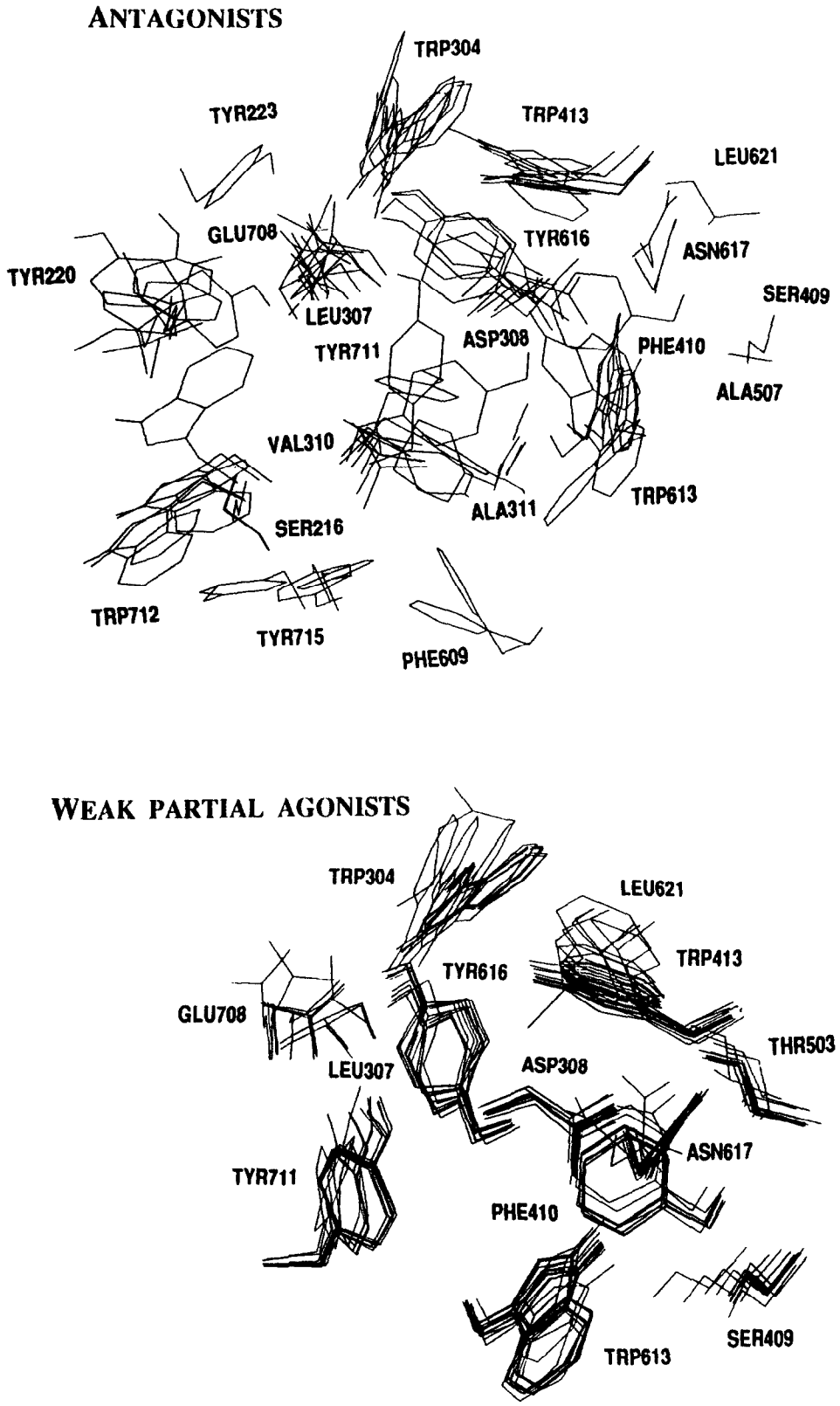
ANTAGONISTS
TRP304
TYR223
TRP413
LEU621
GLU708
TYR616
ASN617
TYR220
SER409
LEU307
ASP308
TYR711
PHE410
ALA507
VAL310
ALA311
TRP613
SER216
TRP712
TYR715
PHE609
WEAK PARTIAL AGONISTS
TRP304
LEU621
TYR616
TRP413
GLU708
THR503
LEU307
ASP308
ASN617
TYR711
PHE410
SER409
TRP613

Figure 4.

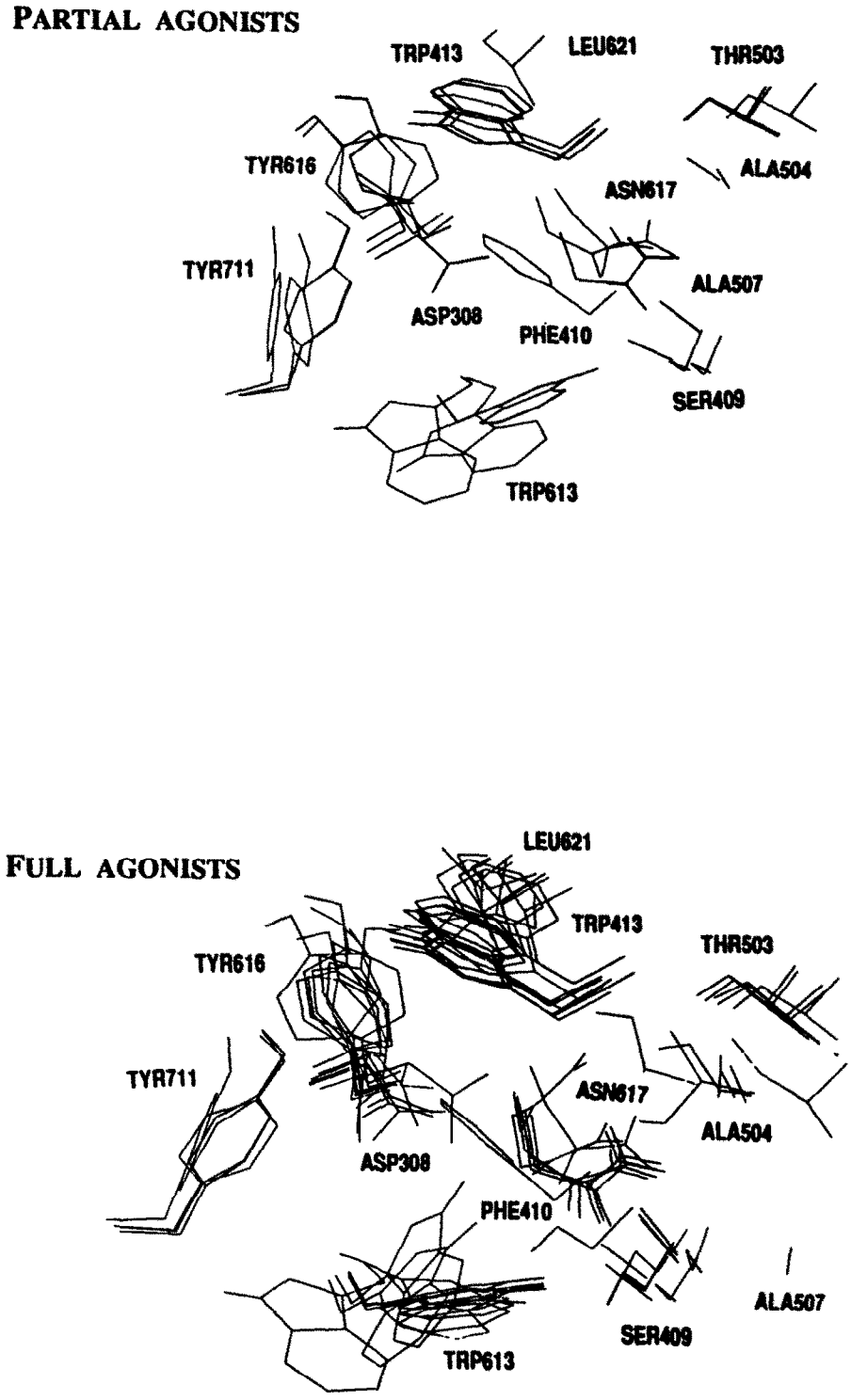

Figure 4. Maps of the m1-receptor binding domain of the antagonists (a), weak partial agonists (b), partial agonists (c) and full agonists (d), obtained by superimposing the selected interacting receptor residues in the same conformation and position they assume in the minimized complexes with the ligands.

(c) The achievement of a good geometry for the H-bonding interaction between the protonated nitrogen atom of the weak partial agonists and Asp_{308} strongly influences the orientation of the rest of the molecule, which is, in general, oriented toward helix 6 and makes π–π stacking or van der Waals attractive interactions with Trp_{413}.
(d) The partial agonists considered in this study are protonated species whose substituents are directed toward helix 5, and make H-bonding interactions with Thr_{503} and Asn_{617}.
(e) The trimethylammonium or the protonated quinuclidine moieties of the full agonists are surrounded by the same aromatic cluster (Trp_{304}, Trp_{413} and Trp_{613}) as in the case of antagonists. Two of these residues (Trp_{413} and Trp_{613}) were also found to be part of a similar aromatic cluster in the m2-model proposed by Trumpp-Kallmeyer *et al.* [14] Furthermore, the small hydrophilic substituent of the trimethylammonium or of the protonated quinuclidine moieties gives two H-bonding interactions with Thr_{503} and Tyr_{616} or with Thr_{503} and Asn_{617}. The last pair of residues is involved in two H-bonding interactions also in the agonist-human m1-model recently proposed by Nordvall and Hacksell.[15] The amino acid composition of the binding site model proposed by these authors is similar to the agonist binding domain of our model, although the procedure they utilized for its definition is quite different.[15] Moreover, a general agreement on the interacting points between the receptor and the three agonists (**14**, **31** and **32**) which are in common is observed; the only differences are: the carbonyl group of oxotremorine (**31**) in our model acts as H-bonding acceptor with respect to the residues Thr_{503} and Asn_{617}, whereas in the model of Nordvall and Hacksell it is proposed to make only one H-bond with Asn_{617};[15] the Thr_{503}-Tyr_{616} pair of residues makes two H-bonds with muscarine (**32**) in our model, whereas, in the model of these authors, the same interactions are accomplished by the Thr_{503}–Asn_{616} pair:[15]
(f) The extent of the interaction with Asp_{308} negatively influences the interaction of the same ligand with Thr_{503}. Thus, a quaternary nitrogen atom, which gives an ionic interaction with Asp_{308} usually weaker than the charge reinforced H-bonding one, together with a small hydrophilic substituent, able to make at least two intermolecular H-bonding interactions with Thr_{503} and Tyr_{616} or with Thr_{503} and Asn_{617}, may be an important structural determinant for the expression of the full agonist action.

Conclusions

Theoretical QSAR analysis has been accomplished on 3D-models of 34 ligands–m1 muscarinic receptor complexes. We have used the results from site-directed mutagenesis experiments in order to determine the binding preferences of the ligands. In this context a model with different but overlapping binding sites for the agonists and the antagonists seems to be more realistic than a single site model. Good linear correlations have been obtained between ad hoc theoretical intermolecular interaction descriptors and the pharmacological action, which allow one to classify quantitatively and predict the pharmacological action of new ligands. In particular, antagonists show $IE_{(HB+EL)}$% values below or close to 20%, full agonists show $IE_{(HB+EL)}$% values above 30%, whereas weak partial and partial agonists show $IE_{(HB+EL)}$% values in between the previous two. These results are in agreement with the pharmacological model recently proposed by Saunders *et al.*[32] and with our previous theoretical indirect QSAR models.[1] Finally, the computation of the energy contributions of each amino acid residue to the total *IE* has allowed the identification of the protein residues mainly involved in the interaction with the ligands. In our opinion, the heuristic-direct QSAR approach presented, although quite elaborated from a molecular modelling point of view, shows some advantages over the traditional QSAR approaches. In fact, it is based on the 3D-chemical formalism which is relatively easy to handle and universally understood also for complex macromolecular structures. Moreover, the 3D-chemical formalism applied to the receptor description provides a quantitative and consistent tool for comparisons among the different transmembrane receptors and suggests, on a formal basis, site directed mutagenesis experiments, which, in turn, might support or confute the model proposed. In this way also, receptor structure affinity–selectivity relationships can be comparatively elucidated. On this correlative ground the drastic simplifications and approximations introduced in the receptor model building procedure become more acceptable.

Experimental Section

Computational methodology

Modelling studies have been performed with the molecular package QUANTA (version 3.3.1).[33] Energy minimizations of the receptor and of the complexes have been achieved by means of the program CHARMm (version 22).[34]

Minimizations have been carried out on an HP-720 workstation by using the conjugate gradient minimizer, until the rms gradient was less than 0.01 kcal/mol Å. A distance dependent dielectric term ($\varepsilon = 4r$) and a 12 Å atom based cutoff distance have been chosen. An 'all atom' force field representation has been used for the ligands while, in the case of the receptor, the hydrogens bonded to carbon atoms have not been explicitly included ('united atom approximation') for computational efficiency.[34] The interaction energies (*IE*) of the ligand–receptor minimized complexes have been computed according to the following formula: $IE = E_{COMPLEX} - E_{REC} - E_{LIG}$, where $E_{COMPLEX}$ is the energy of the ligand–receptor minimized complex, E_{REC} and E_{LIG}, are the energies of the receptor and of the ligand, respectively, in the minimized complex. The *N*-methylscopolamine has been obtained by adding hydrogens and the *N*-methyl group to the crystal structures of (–)-scopolamine hydrobromide;[35] atropine has been obtained by adding hydrogens and by changing all signs to the original coordinates of the hydrochloride enantiomer.[36] Muscarine, pilocarpine and pirenzepine have been obtained

from the crystal structures of (+)-muscarine iodide, (+)-pilocarpine hydrochloride and pirenzepine monohydrochloride, respectively.[37–39] The other ligands have been constructed by taking the geometric parameters from standard compilations.[40] The fully optimized geometries of the ligands in their protonated or quaternary forms and their atomic charge distributions have been obtained in the AM1 framework.[41] The ligand atoms have been assigned the parameters of the corresponding CHARMm atom types.[34]

Acknowledgements

Financial support from the Consiglio Nazionale delle Ricerche (Roma) and Ministero dell' Università e della Ricerca Scientifica (funds 40%) is acknowledged.

References

1. Fanelli, F.; Menziani, M. C.; Carotti, A.; De Benedetti, P. G. *J. Mol. Struct. (Theochem)* **1993**, *283*, 63.

2. De Benedetti, P. G.; Menziani, M. C.; Fanelli F.; Cocchi, M. *J. Mol. Struct. (Theochem)* **1993**, *285*,147.

3. Nathanson, N. M. *Ann. Rev. Neurosci.* **1987**, *10*, 195.

4. Strosberg, A. D. *Eur. J. Biochem.* **1991**, *196*, 1.

5. Savarrese, T. M.; Fraser, C. M. *Biochem. J.* **1992**, *283*, 1; and references therein.

6. Wess, J. *Life Sci.* **1993**, *53*, 1447; and references therein.

7. Peralta, E.; Ashkenazi, A.; Wilson, J. W.; Smith, D. H.; Ramachandran, J.; Capon, D. J. *EMBO J.* **1987**, *6*, 3923.

8. Hulme, E. C.; Birsdall, N. J. M.; Buckley, N. J. *Ann. Rev. Pharmacol. Toxicol.* **1990**, *30*, 633.

9. Mutschler, E.; Moser, U.; Wess, J.; Lambrecht, G. In *Prog. Pharmacol. Clin. Pharmacol.*, Vol. 7/1, pp. 13–31, Gustav Fischer Verlag; Stuttgart, 1989.

10. Buckley, N. J.; Bonner, T. I.; Buckley, C. M.; Brann, M. R. *Mol. Pharmacol.* **1989**, *35*, 469.

11. Freedman, S. B.; Harley, E.; Iversen, L. L. *Br. J. Pharmacol.* **1988**, *93*, 437; and references therein.

12. Findlay, J.; Eliopoulos, E. *Trends Pharmacol. Sci.* **1990**, *11*, 492.

13. Hibert, M. F.; Trumpp-Kallmeyer, S.; Bruinvels, A.; Hoflack, *J. Mol. Pharmacol.* **1991**, *40*, 8.

14. Trumpp-Kallmeyer, S.; Hoflack, J.; Bruinvels, A.; Hibert, M. F. *J. Med. Chem.* **1992**, *35*, 3448.

15. Nordvall, G.; Hacksell, U. *J. Med. Chem.* **1993**, *36*, 967.

16. Brann, M. R.; Klimkowski, V. J.; Ellis, J. *Life Sci.* **1993**, *52*, 405.

17. Blundell, T.; Barlow, D.; Borkakoti, N.; Thornton, J. *Nature* **1983**, *306*, 281.

18. Henderson, R.; Baldwin, J. M.; Ceska, T. A.; Zemlin, F.; Beckmann, E.; Downing, K. H. *J. Mol. Biol.* **1990**, *213*, 899.

19. Sankuratri, S.; Von Zastrow, M.; Kobilka, B. K. *J. Biol. Chem.* **1992**, *267*, 21991.

20. Baldwin, J. M. *EMBO J.* **1993**, *12*, 1693; and references therein.

21. Schertler, G. F. X.; Villa, C.; Henderson, R. *Nature* **1993**, *362*, 770.

22. MaloneyHuss, K.; Lybrand, T. P. *Mol. Biol.* **1992**, *225*, 859.

23. Ponder, J. W.; Richards, F. M. *J. Mol. Biol.* **1987**, *193*, 775.

24. Cronet, P.; Sander, C.; Vriend, G. *Protein Engng.* **1993**, *6*, 59.

25. Hulme, E. C.; Kurtenbach E.; Curtis, C. A. M. *Biochem. Soc. Transact.* **1991**, *19*, 133.

26. Drubbisch, V.; Lameh, J.; Philip, M.; Sharma, Y. K.; Sadee, W. *Pharm. Res.* **1992**, *9*, 1644.

27. Lewell, X. Q. *Drug Design and Discovery* **1992**, *9*, 29.

28. Tota, M. R.; Strader, C. *J. Biol. Chem.* **1990**, *265*, 16891.

29. Jasper, J. R.; Insel, P. A. *Biochem. Pharmacol.* **1992**, *43*, 119.

30. Saunders, J.; Cassidy, M.; Freedman, S. B.; Harley, E. A.; Iversen, L. L.; Kneen, C.; MacLeod, A. M.; Merchant, K. J.; Snow, R. J.; Baker, R. *J. Med. Chem.* **1990**, *33*, 1128.

31. Cocchi, M.; Menziani, M. C.; De Benedetti, P. G.; Cruciani, G. *Chemometrics Intell. Lab. Syst.* **1992**, *14*, 209.

32. Saunders, J.; Freedman, S. B. *Trends Pharmacol. Sci. Suppl.* **1989**, 70.

33. QUANTA/CHARMm, 1990, Polygen Corporation, 200 Fifth Avenue, Waltham, MA 02254.

34. Brooks, B. R.; Bruccoleri, R. E.; Olafson, B. D.; States, D. J.; Swaminathan, S.; Martin, K. *J. Comput. Chem.* **1983**, *4*, 187.

35. Glaser, R.; Charland J.-P.; Michel, A. *J. Chem. Soc. Perkin Trans. II* **1989**, 1875.

36. Kussaether, E.; Haase, J. *Acta Crystallogr., Sect. B* **1972**, *28*, 2896.

37. Jellinek, F. *Acta Crystallogr.* **1957**, *10*, 277.

38. Codding, P. W.; James, M. N. G. *Acta Crystallogr., Sect. B: Struct. Sci.* **1984**, *40*, 429.

39. Trummlitz, G.; Schmidt, G.; Wagner, H.-U.; Luger, P. *Arzneim.-Forsch./Drug Res.* **1984**, *34*, 849.

40. Landolt–Bornstein Structure Data of Free Polyatomic Molecules, Vol. 7; Springer-Verlag; Berlin, 1976.

41. Dewar, M. J. S.; Zoebisch, E. G.; Healey, E. F.; Stewart, J. J. P. *J. Am. Chem. Soc.* **1985**, *107*, 3902.

(*Received* 24 *November* 1993; *accepted* 1 *February* 1994)